AJEMA GLOBAL RESEARCH NETWORK

AMERICAN Journal of Engineering, Mechanics and Architecture
Volume 4, Issue 03, 2026 ISSN (E): 2993-2637

Experimental Investigation of Heating Element Performance with Bypass Tubes

Saad H. Saadoon
Department of Mechanical Engineering, University of Misan, Misan, Iraq
Department of Mechanical Engineering, Mustansiriyah University, Baghdad, Iraq

Mohammed H. Alhamdo
Department of Mechanical Engineering, Mustansiriyah University, Baghdad, Iraq

Abstract: This study presents an investigation of the thermo-hydraulic performance of a rotary air preheater heating element utilizing bypass tubes and wire coiled coil matrix turbulators. The work purpose is to improve heat transfer efficiency and minimize flow resistance while considering the practical problems observed in failed heating elements utilized in industrial units such as the Al-Hartha Thermal Power Station in southern Iraq. The experimental setup is intended for simulating working conditions of an air preheater under cyclic charging and discharging of hot and cold air flows. Air from a single matrix is switched between the two directions of flow using a valve-controlled system driven by an automated control panel. Three different types of bypass layout are tested in order to determine the best positioning and number of the tubes. Additionally, bypass tubes with various diameters (10, 15 and 20 mm) and shapes (circular and squared section) are tested. Also, three turbulators with different pitches are inserted into the bypass tubes to increase turbulence and enhance convective heat transfer. The results clarify the interlinked influences of bypass flow control and turbulent augmentation on the overall performance of stack heat recovery elements. The thermo-hydraulic performance for inline-tube arrangement rises on the order of 7.58% over the conventional element, while the 15 mm tubes deliver improvement of 15.47%. The cylindrical section outperformed the square section over examined Re range, with an improvement 23.49%, while the 5 mm pitch turbulator achieved an improvement of 23.92%.

Keywords: Air preheater, Power plant, hydro-thermal performance, bypass tubes, turbulator, heating element.

1. Introduction

Experimental studies of Rotary Air-Preheaters (RAPHs) have helped to understand the intricate connection between heat transfer enhancement, flow resistance, and structural design optimization. Early research including that of Ghodsipour and Sadrameli [1] and Skiepko and Shah [2] established important correlations between theoretical and measured performance in large-scale laboratory rotary heat exchangers. Their work demonstrated that the theoretical regenerator models could predict overall performance to an accuracy of ±5% under controlled conditions but their geometry was simplified and did not account for local flow maldistribution or transient in the matrix structure.

Later experiments, such as that of Wang et al. [3] and Akbari et al. [4], presented in more advanced test rigs integrating honeycomb ceramics and corrugated metallic matrices for a more

realistic simulation of industrial RAPHs. The results revealed as much as 10-15% improvements in thermal effectiveness via geometry optimization. However, their configurations were restricted to fixed range Reynolds numbers and steady-state conditions, failing for accounting actual transient nature of the flow reversal and leakage that is part of life when dealing with rotating matrices. Further, with respect to experimental results, the absence of common performance metrics limited the ability for inter-comparison among cases.

Recent experimental attempts, such as those detailed by Hazim [5] and White [6], have greatly improved upon the experimental methodology, utilizing full-scale rigs and optimization methods. Hazim carried out its design with a 0.9 m test section and modular baskets that provided a robust platform for studies on Double Undulated (DU) elements and the effect of bypass tubes on flow uniformity. This study filled the gap between CFD predictions and operating conditions, it showed an observable improvement in Nusselt number as well as pressure drop performance. However, even with these advances, the bulk of the available experiments had concentrated on specific shapes and not come up with a generalized correlation that could be useful for different RAPHs.

With respect to materials and geometry, Zhu [7] and Yu [8] offered important contributions regarding the impact of corrugation design and notching on heat transfer efficiency demonstrating that the corrugation angle and pitch ratio significantly affect turbulence intensity as well as reattachment mass flow. However, their tested sections were still too small and the simplified air channels restricted scalability to industrial settings. Similarly, Zhang et al. [9] give precious experimental results about temperature profile and corrosion effects in preheater stages of industrial size plants but concentrating more on thermal homogeneity than on detailed flow or heat transfer maps.

In general, there has been significant advancement in the experimental research of matrix geometry, flow resistance and thermal effectiveness, yet several limitations persist. The present study focuses on the experimental investigation to verify the thermo-hydraulic performance of heating element with a bypass tubes. In the present work, influence of different bypass tubes patterns, geometry and size on heat enhancement, pressure drop characteristics along with performance index of the element has been studied. Through the systematic study of different arrangements with controlled airflow, is aimed to identify the best by-pass design that achieves the optimal trade-off between increased heat transfer and reduced flow resistance. Turbulators are also used to enhance heat transfer, such as a Wire Coiled Coil Matrix Turbulator (WCCMT) placed within the heating medium. Finally, the results are anticipated to aid in the design of higher efficiency heat elements for rotary air preheaters and like heat recovery systems.

2. Experimental approach.

2.1. experimental setup

The (RAPH) represents a periodic-type heat exchanger that can operate in two main arrangements, the rotating (spinning) form and the switching form. With the mass flow correlation between these two configurations, a general design framework of periodic heat exchangers can be constructed [10]. In the present study, the valve-controlled switching mode was utilized for the RAPH, and comparative experiment research on thermal-hydraulic performance of the RAPH has been conducted. Unlike the conventional switching design that employs two distinct heat storage cores, the current configuration utilized a single heat transfer matrix through which the alternating flow of hot and cold air was achieved by an automated solenoid valve system. This kind of mechanism allowed controlling the charging and discharging cycles in one ‘matrix’, thus mimicking a regenerative heat exchange process. The experiments were conducted in a hot air wind tunnel which was built on purpose for this procedure. The experimental setup is illustrated in Figure 1, and corresponding schematic diagram are shown in Figure 2. The entire wind tunnel is 7780 mm long, in which the cross section of test chamber is

250 × 250 mm and a cylindrical section diameter of 63.5mm, to ensure that the airflow distribution is stable and uniform during throughout experiment region.

To minimize heat loss, the wind tunnel was constructed using 1 mm thick galvanized steel and thermally insulated with a 5 cm layer of glass wool having a thermal conductivity of K = 0.04 W/m·K.

The heat transfer element test box is 940 mm in length and has a 250*250 mm rectangular cross section area. It consists of three layers, cold intermediate, and hot layers, the specifications of the three layers are given in Table 1. The high temperature flue gas employed in this work was generated from heated air by an electrical heater. Five electrical heaters are used with capacity each of 5000 W. The cold air is the ambient temperature. During the experimental operation, the flow of hot and cold air through the system was controlled automatically using a dedicated control system, as illustrated in Figure 3-a. This system managed the sequential opening and closing of the five solenoid valves, as illustrated in Figure 3-b, according to the selected charging and discharging periods. At the beginning of the heating cycle, valves No.1, No.3, and No.5 are opened to allow hot air to pass through the heating matrix, while valves No. 2, and No. 4 are closed in a predefined sequence to guarantee the protection and stability of the equipment. The heated air was charged through the matrix and exited from valve No. 5 without interfering with the flow of cool air through the system. After the charging process finished, the control system switched to the discharging period when valves No.2, No.3, and No.4 were opened and then valves No. 1 and No. 5 turned off step. This automatic transfer resulted in the release of heat stored in the matrix, with hot air being expelled through valve No. 3 for smooth, efficient discharging period operation. The experimental procedure was repeated until steady-state conditions were reached. The temperature, pressure and velocity were measured for each run systematically. Temperature measurement was done using K-type thermocouples with a range of 0-1300°C and an accuracy of ±0.4%, as illustrated in Figure 4-c. These thermocouples were positioned along the length and at the ends of the tunnel to record the inlet and outlet air temperatures, as illustrated in Figure 4-a and Figure 4-d. A total of twenty-five temperature measurement points were evenly distributed across the cross-sections of the test section, as shown in Figure 4-b. The average readings from repeated measurements were used to determine the bulk fluid temperature. The end-wall temperature of the heat transfer elements were measured using the same thermocouple arrangement. For the bypass configurations, the thermocouples were mounted through thin-walled bypass tubes inserted into the heating element channels to record local temperature variations. Pressure measurements were taken using a pressure transmitter with an uncertainty of ±0.25%, while airflow velocity was measured using a hot-wire anemometer with an error margin of ±0. 9%. The operational ranges of the key experimental parameters are summarized in

Table 2. All measurement signals were conveyed to an individual computer via a data acquisition system, with a sampling interval of 1 second to ensure precise temporal resolution of the recorded data.

Figure 1.Experimental system

1. Blower	2. Pneumatic valve No.1	3. Pneumatic valve No.2	4. Pneumatic valve No.3
5. Diffuser	6. Data loggers	7. Pressure sensor	8. Test section
9. Thermocouples	10. Anemometer	11. Pneumatic valve No.4	12. Nozzle
13. Pneumatic valve No5	14. Pipe	15.Electric source	16. Pneumatic control system

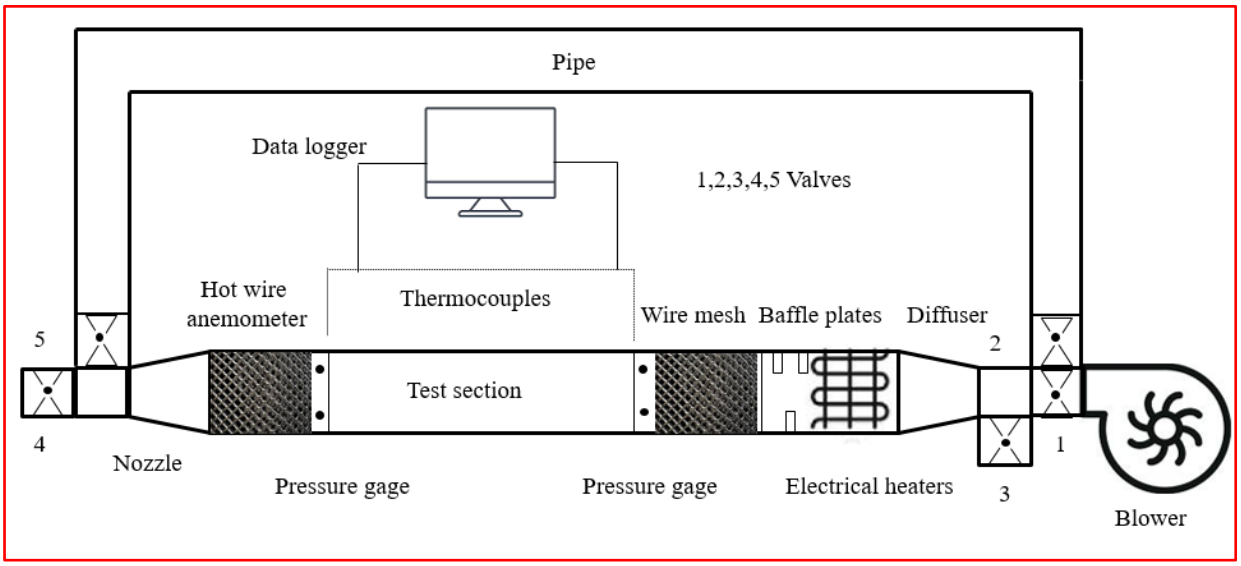

Figure 2. Schematic diagram of the experimental system

a b

Figure 3.Control system of solenoid valves.(a) control panel (b) solenoid valve

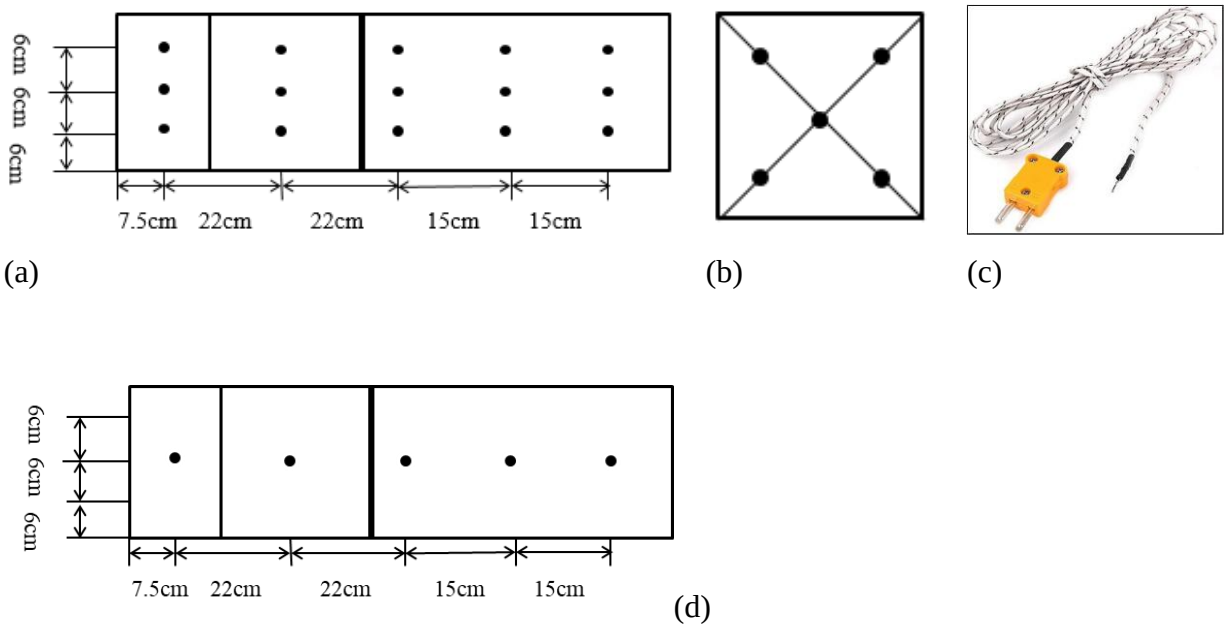

Figure 4.Thermocouples distribution (a) along the test section (b) at the outlet and inlet of the test section (c) thermocouple(d) the top distribution

Table 1. Material properties of heating elements [11]

Thermal conductivity (W/m.K)	Specific heat(J/kg.K)	Density (kg/m^3)	Material	Layer
25	460	7700	Mild steel	Cold & intermediate
54	465	7833	Corten steel	Hot

Table 2. Experimental parameters ranges

Parameter	Unit	Value

Hot side air	k	340
Cold side air	k	300
Re	dimensionless	500-10500
Charge and discharge period	s	10

2.2. The geometry and thermal hydraulic properties

During the field inspection conducted at the Al-Hartha thermal power plant in Basra, southern Iraq, a significant level of deterioration was observed in the heating element matrix of the rotary air preheater, as shown in Figure 5. The failed matrix presented surface oxidation, material cracking and plate warping as a consequence of long-term interaction with high flue gas temperatures, fly ash corrosion and thermal cyclic fatigue. The once uniform corrugation of heating elements had become visibly distorted, resulting in reduced heat transfer surface area, non-uniform air passage and excessive pressure drop across the preheater sector. On the contrary, the Notched Flat (NF) heating element that was offered by general company for inspection and rehabilitation of electrical systems in Baghdad, Iraq shown in Figure 6, depicts an undamaged heating element with well-defined corrugation geometry and a clean, intact metallic surface. This arrangement will result in a more uniform air flow distribution and better convective heat transfer, as well as less of the hydraulic resistance of the matrix. The comparison between the deteriorated and pristine surfaces demonstrates the significant effect of material deterioration on heat-hydraulic performance. The resulting damage could also aid in flow non-uniformity and poor heat recovery and a quantifiable loss of boiler efficiency. The heating element layers specifications are detailed in Table 3

This experiment result indicates that periodic check and replacement of corroded components for the running RAPH units are essential to maintain their thermal performance effectively and prevent system imbalanced. It is also used as the reference for laboratory-scale assessments, trying to reproduce real aging effects under controlled operating conditions.

The bypass part of the experimental rig consisted of a series of stainless steel tubes with varying cross-section geometry and hydraulic diameter, each designed to study how shape and size affect fluid flow behavior as well as pressure characteristics. Three cylindrical tubes are utilized with internal diameters of 10 mm, 15 mm, and 20 mm Besides the circular tubes, a square tube b is also applied and designed with an identical cross-sectional area of that of 15 mm diameter circular pipe. Therefore guaranteeing that a fair comparison between the two geometries for similar flow conditions can be made, as illustrated in Figure 7. Initially, three different arrangements could be prepared in the experiment, staggered arrangement with 15 tubes, staggered arrangement with 17, and an inline arrangement with 21 tubes, as shown in Figure 8. The same corrugated heating element matrix was used for all, but the number and arrangement of bypass tubes incorporated in the assembly differed between that of each configuration. An extra test condition was carried out to assess the influence of tube diameter on the global thermal-hydraulic performance of notched flat heating element. The three tube sizes (10 mm, 15 mm and 20 mm diameter) were considered to find the optimum arrangement that gives the best compromise between heat transfer augmentation and flow resistance, as illustrated in Figure 9. At this stage a square tube was added and designed to have the same cross-sectional area as the 15mm circular tube for comparison purposes (not flow area comparison), as illustrated in Figure 10. Under current experimental condition, wire coiled coil matrix turbulators (WCCMTs) were installed in the heating element matrix of rotary air preheater (RAPH), where the heat transfer performance was improved and which is conducive to cleanliness of cleaning for a matrix. To the best of the authors' knowledge, no previous studies have experimentally investigated the use of WCCMTs within RAPH matrices. In this work, three different WCCMT configurations were

fabricated and tested, as shown in

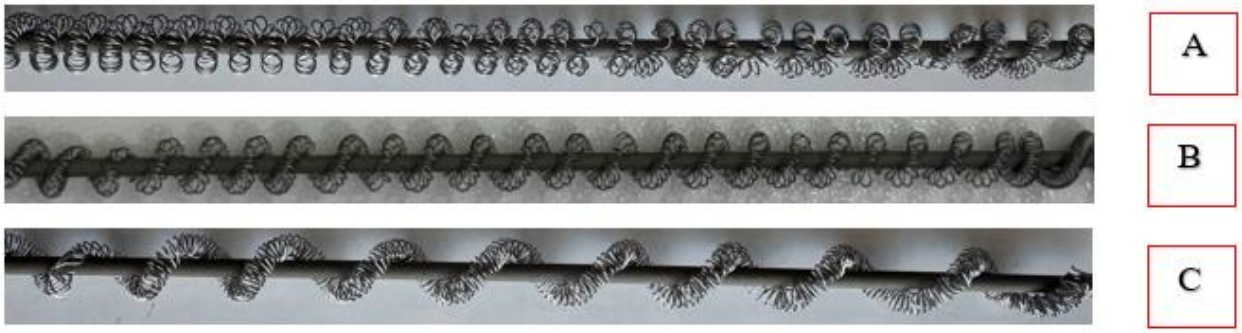

Figure 11. Each turbulator was designed as a modified wire-mesh insert, consisting of a fine steel wire wound helically around a central rod to induce a swirling motion of air within the flow passage.

The WCCMTs were manufactured by uniformly winding a 0.7 mm diameter steel wire around a 5 mm diameter steel rod to produce three different pitches (5 mm, 10 mm, and 15 mm). For the 5 mm pitch, approximately 80 turns of the wire were wound over a 420 mm rod, followed by soldering along the interface to eliminate any air gaps between the wire and the rod. The same procedure was applied for the other two pitches, yielding 40 turns for the 10 mm pitch and 25 turns for the 15 mm pitch. The geometric specifications of the three WCCMT configurations are summarized in Table 4, and the detailed structural representation is illustrated in Figure 12

Finally, the bypass matrix equipped with the insert is illustrated in Figure 13.

Figure 5.Damaged heating elements

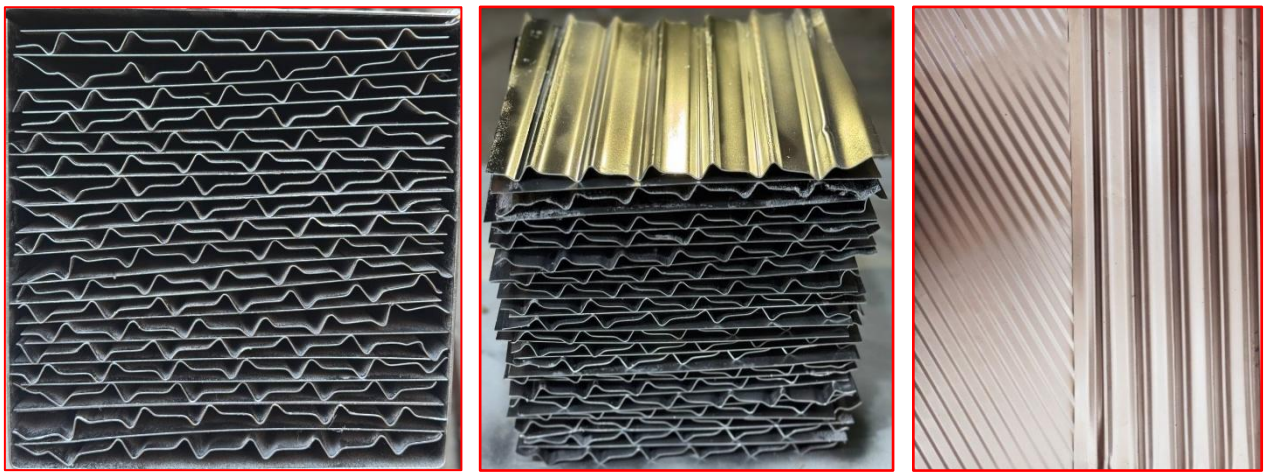

Figure 6.Geometric of heat transfer element

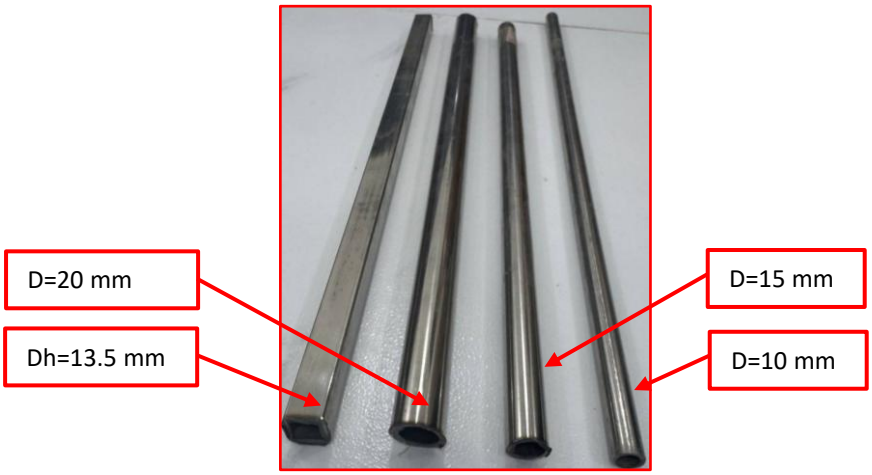

Figure 7.Bypass tubes

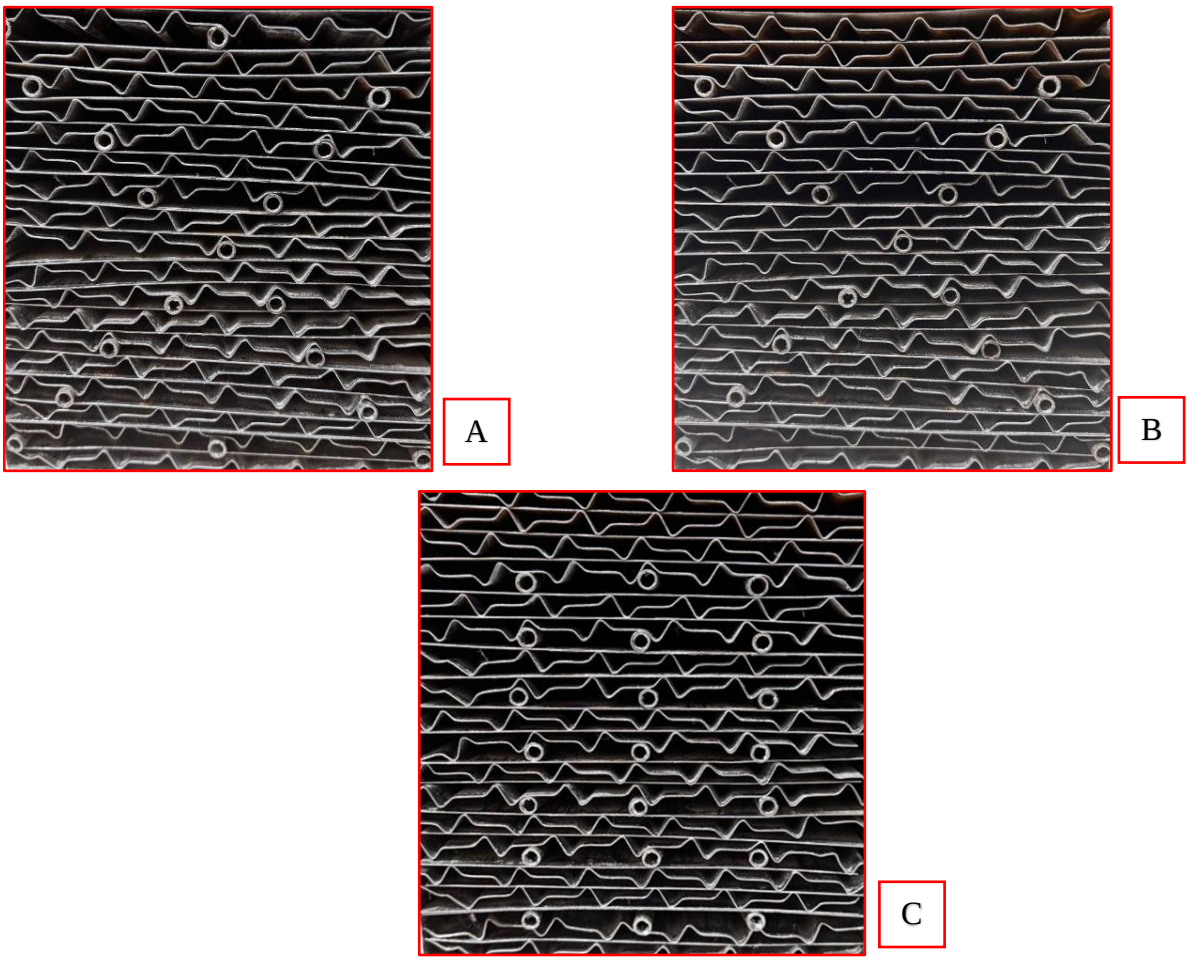

Figure 8. Bypass matrix (A) staggered arrangement with 15 tubes (B) staggered arrangement with 17 tubes (C) inline arrangement with 21 tubes

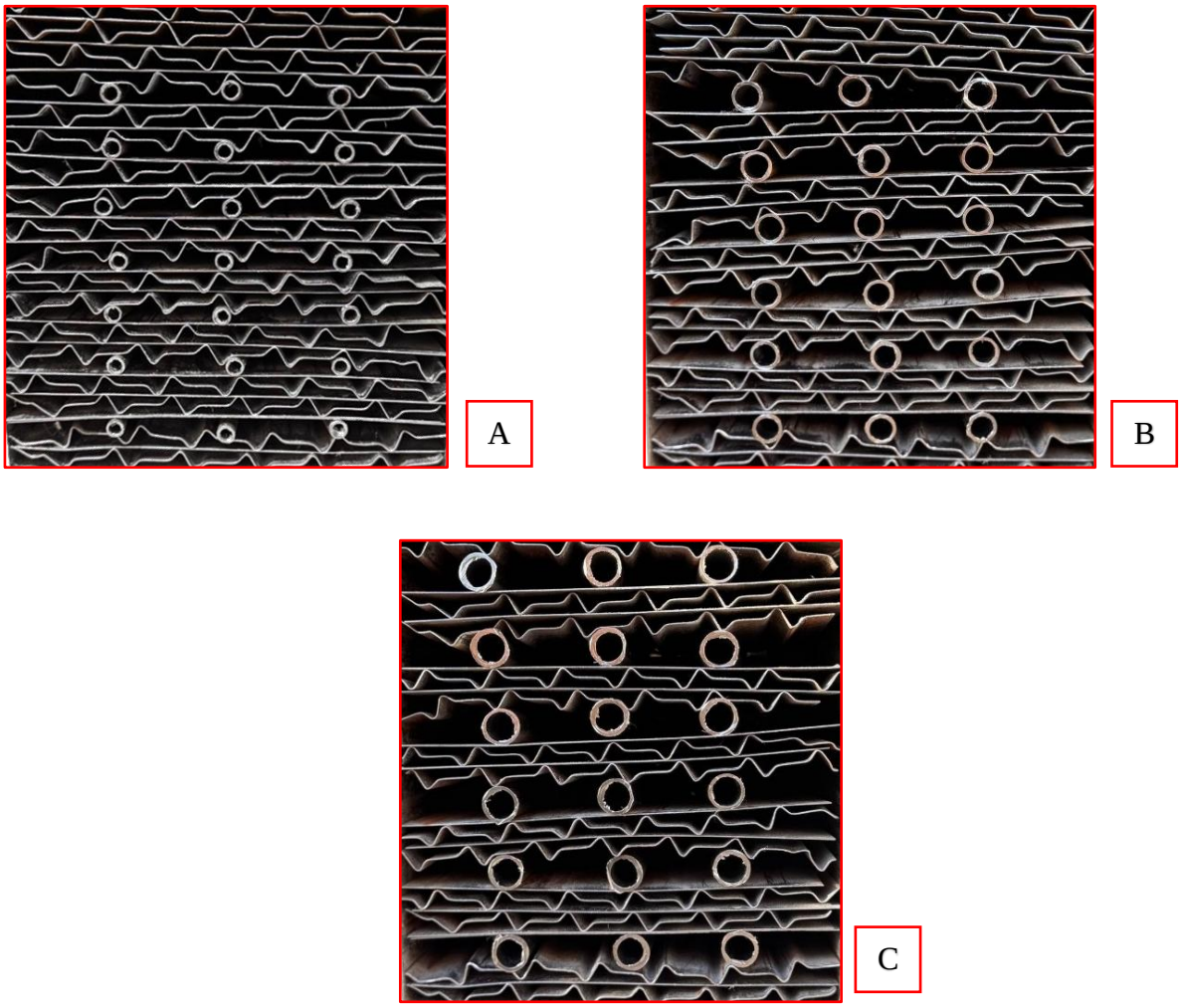

Figure 9. Bypass matrix at different bypass tube diameters (A) D=10 mm (B) D= 15 mm (C) D= 20 mm

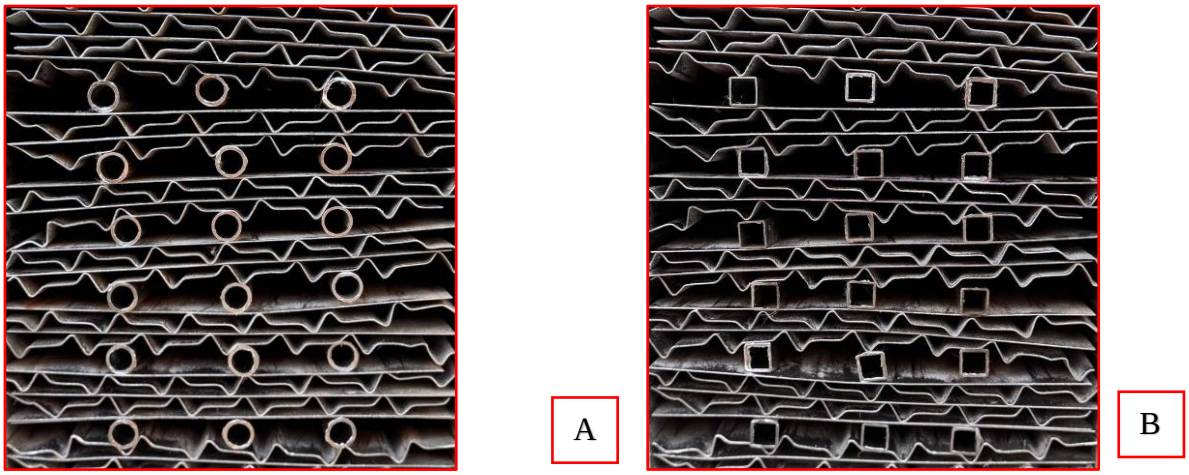

Figure 10. Bypass matrix at different bypass tubes cross section area (A) cylindrical (B) square

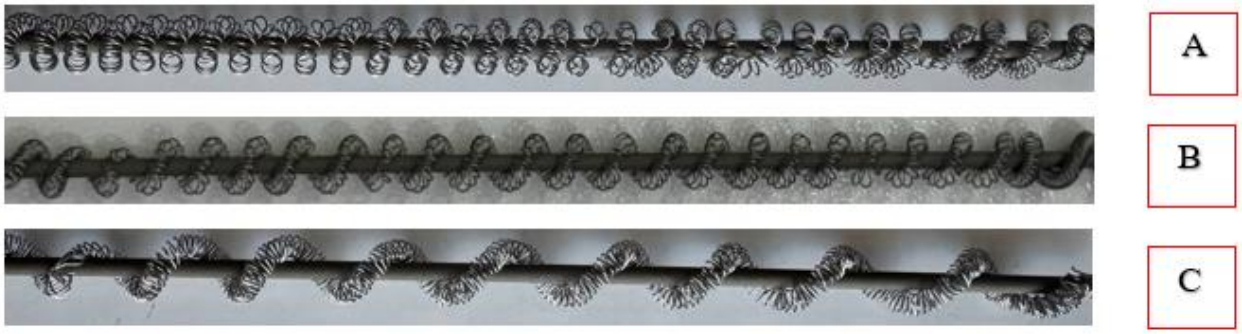

Figure 11. The WCCMT different configuration (A) pitch 5 mm (B) pitch 10 mm (C) pitch 15 mm

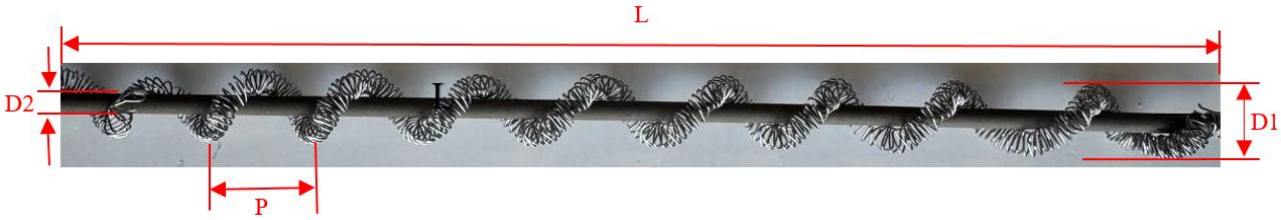

Figure 12. The WCCMT details

Figure 13.Bypass matrix with insertion

Table 3. Specifications of heating element layers [11][12]

Characteristics	Hot layer	Intermediate layer	Cold layer
Profile	NF	NF	NF
Thickness(mm)	0.8	1.2	1.2
Height(mm)	500	250	150
Material	Mild steel	Corten steel	Corten steel

Table 4. The geometric specifications of the three WCCMT configurations

Configuration	Length (L) (mm)	Pitch (P) (mm)	Diameter of the WCCMT (D1) (mm)	Diameter of the shaft (D2) (mm)	Number of turns
Ins.1	420	5	14	5	80
Ins.2	420	10	14	5	40
Ins.3	420	15	14	5	25

The collected experimental data from the tests will be utilized to develop empirical correlations for Nu and *f*. These correlations are formulated based on the characteristic velocity, which serves as the defining parameter and is expressed as follows:

$$u = \frac{\dot{m}}{\rho A_{c,ch}} \quad (1)$$

Where: $\dot{m}$ represents the fluid mass flow rate, ρ is the density of the fluid, and $A_{c,ch}$ denotes the channel's cross-sectional area. The characteristic velocity corresponds to the ratio between the upstream fluid velocity and the porosity of the heat transfer surfaces. However, the estimate of fluid density in this context based on the local temperature. Using the characteristic velocity and the equivalent diameter, the Reynolds number-a key dimensionless parameter describing the flow regime-can then be determined.

$$Re = \frac{\rho u D_h}{\mu} \quad (2)$$

Where Dh is an equivalent diameter, μ is the dynamic viscosity of the fluid;

2.3. Performance parameters

The pressure drop is a crucial parameter governing the fluid flow process. To express it in a dimensionless form, the equivalent friction factor is defined to characterize the flow resistance within the system.

$$f = \frac{2\Delta p D_h}{\rho_f u_f^2 L} \quad (3)$$

Where: Δp is the pressure drop, produced by the passages of fluids around the heat transfer surfaces. L represent the length of the heat transfer section=940 mm in all experiments.

The rate of the heat transfer in the discharge period that are flowing through the test section can be determined by using the following equations [13].

$$\dot{Q} = \dot{m} C_p (T_o - T_i) \quad (4)$$

Where: C_p is specific heat

The convection heat transfer coefficient is a vital performance indicator for heat exchangers, reflecting the intensity and efficiency of convective heat transfer between the fluid and the heat transfer surface. The average convective heat transfer coefficient for the entire heat exchanger can be determined using Newton's law of cooling, which is expressed as follows [14]:

$$\bar{h} = \frac{\dot{Q}}{A_s (T_{s,ave} - T_m)} \quad (5)$$

Here $T_m = \frac{T_o + T_{in}}{2}$ (6)

$$T_{s,ave} = \frac{1}{15} \sum_{i=1}^{15} T_{s,ave,i} \quad (7)$$

Where: A_s represents the effective heat transfer area of the heating elements. The effective area is 30 m² the metal corrugated plate matrix and 25 m² for bypass matrix. Since the convective heat transfer coefficient depends on multiple complex factors, it is expressed in terms of the dimensionless Nusselt number (Nu). Consequently, the Nusselt number can be determined using the corresponding thermos-physical properties of the working fluid [15].

$$Nu = \frac{\bar{h} D_h}{k} \quad (8)$$

Here, k denotes the thermal conductivity of the fluid. The expression above is accepted as an engineering performance parameter adequately portraying heat transfer capability of the system [16].

The Culborn j-factor is defined as [17]:

$$j = \frac{Nu}{PrRe^{0.5}} \quad (9)$$

Where: Pr is Prandtle number.

The overall thermal and hydraulic performance of the RAPH is estimated based on a Performance Index Factor (PIE) comparing the improved heat transfer and flow resistance properties of the novel models to those of the baseline concept at equal pump power conditions [18].

$$PIF = \frac{Nu}{f^{1/3}} \quad 10$$

And finally, the Performance Evaluation Factor (PEF) is given by equation 11

$$PEF = \frac{\frac{Nu_{mod.}}{Nu_{conv.}}}{\left(\frac{f_{mod.}}{f_{conv.}}\right)^{1/3}} \quad 11$$

2.4. Uncertainty analysis

Precise calculation of the Nusselt number (Nu) is crucial in assessing the convective heat transfer behavior of thermal systems. Because Nu is based on a several of experimentally measured values (e.g. temperature difference, mass flow rate, fluid properties and heat transfer surface area), each associated measurement makes its own contribution to the overall experimental uncertainty. As a result, it is important that the errors associated with these comparisons are not so great as to invalidate trends observed in performance or to become limited by uncertainties. In these experiments the determination of uncertainty was performed as described by Kline and McClintock (1953)[19]. The uncertainty in each of the four basic measurements (temperature, pressure, velocity and flow) was estimated using instrumentation precision limits and calibrated accuracies. The individual uncertainties were then combined via the RSS method through the governing equations to assess uncertainty in the computed Nusselt number. The overall uncertainty in Nu is therefore a combination of instrumental precision and error propagation from dependent factors like the convective heat transfer coefficient and Reynolds number. The analysis gives confidence in the quantitative validity of the experimental results and proves that performance correlations deduced from the study are robust.

The root-sum-square (RSS) technique might incorporate the uncertainty (U) of each independent variable [20] according to equation 8.

$$\frac{U_R}{R} = \frac{1}{R}\left[\sum_{i=1}^{N}\left(\frac{\partial R}{\partial x_i}U_{x_i}\right)^2\right]^{1/2} \quad 12$$

Where: R is the value obtained from the above equation; xi is the independent variable; U is the uncertainty in that variable

Neglecting the impact of thermal radiation on the measured temperature, and from equations 4 and 5, the convection heat transfer coefficient can be introduced as in equation 13.

$$h = \frac{\dot{m}C_p\Delta T}{A_s\Delta T_m} \quad 13$$

Where: ΔT is $(T_o - T_i)$,while ΔT_m is $T_s - T_m$

Also, with equation 8, then the independent measured variables are: $\{\dot{m}, C_p, \Delta T, A_s, \Delta T_m, k, D_h\}$

So, the uncertainty of h is as given in equation 14

$$\frac{U_h}{h} = \left[\left(\frac{U_{\dot{m}}}{\dot{m}}\right)^2 + \left(\frac{U_{C_p}}{C_p}\right)^2 + \left(\frac{U_{\Delta T}}{\Delta T}\right)^2 + \left(\frac{U_{A_s}}{A_s}\right)^2 + \left(\frac{U_{\Delta T_m}}{\Delta T_m}\right)^2\right]^{1/2} \quad 14$$

Then

$$\frac{U_{Nu}}{Nu} = \left[\left(\frac{U_h}{h}\right)^2 + \left(\frac{U_{D_h}}{D_h}\right)^2 + \left(\frac{U_k}{k}\right)^2\right]^{1/2} \quad 15$$

Nevertheless, the resistance coefficient, convective heat transfer coefficient, and Reynolds number could not be assigned precise experimental uncertainties, as their formulations inherently involve multiple physical properties-such as density, specific heat, and flow rate which introduce compounded variability. Since the uncertainties associated with these thermos-physical properties and flow parameters are not directly measurable within the scope of the present setup, their effects were neglected in this analysis. Instead, an illustrative uncertainty estimation based on Equation (7) is presented in Table 2. From this evaluation, it can be inferred that the overall uncertainty of the derived parameters is primarily governed by the measurement accuracies of the experimental instruments and the sensitivity of the dependent variables. Based on the detailed propagation analysis, the uncertainties of the Reynolds number and convective Nusselt number were found to be within ±1% and 2.3% respectively, while the uncertainty of the resistance coefficient remained within ±2 %. These ranges confirm that the obtained results are reliable and fall within acceptable experimental limits for thermal-fluid measurements. Sample of uncertainty analysis is given in equation 16.

$$\frac{U_{\overline{Nu}}}{\overline{Nu}} = \left[\left(\frac{0.01818}{0.007819}\right)^2 + \left(\frac{0.02514}{31}\right)^2 + \left(\frac{-0.0075}{2.69}\right)^2\right]^{1/2} \quad 16$$

Thus, the uncertainty in the average Nusselt number is ± 2.33

3. Results and discussions

3.1. Effect of bypass tubes numbers and arrangement

Figure 14 compares four RAPH-element configurations-baseline (conv.), inline-tube arrangement (21 tubes), and two diagonal-tube layouts (15 and 17 tubes)-over Re=500-10,500.

Inline-tube 21 case sits at the top of the group for almost all Reynolds numbers, which confirms what we saw in the parametric study: a moderate corrugation angle plus tube bypass promotes secondary flows without excessive flow blockage. The inline-tube 21 case performs well, suggesting that introducing more tubes at the entry enhances initial boundary-layer disturbance.

The diagonal-tube cases (15 and 17), (conv.), cases cluster close together, while the inline-21 gives a slightly lower (*f*). In other words, the design that gave the highest (Nu) also avoided the steepest drag increase.

Because PIE penalizes pressure drop only to the (1/3) power, the heat-transfer advantage of the inline-21 designs shows up clearly: it occupies the upper edge of the bars at every (Re), with the inlet-21 layout slightly ahead at high Reynolds numbers.

The results therefore tell that: (i) disturbing the inflow raises (Nu); (ii) doing so without overblocking the passage keeps (*f*) low; and (iii) when both happen together, the thermo-hydraulic performance index rises noticeably-on the order of 11% over the conventional element in this range. For design of rotary air preheaters, this means that well-placed inline /bypass tubes give the best “heat-per-pressure-drop with improvement of 11%.

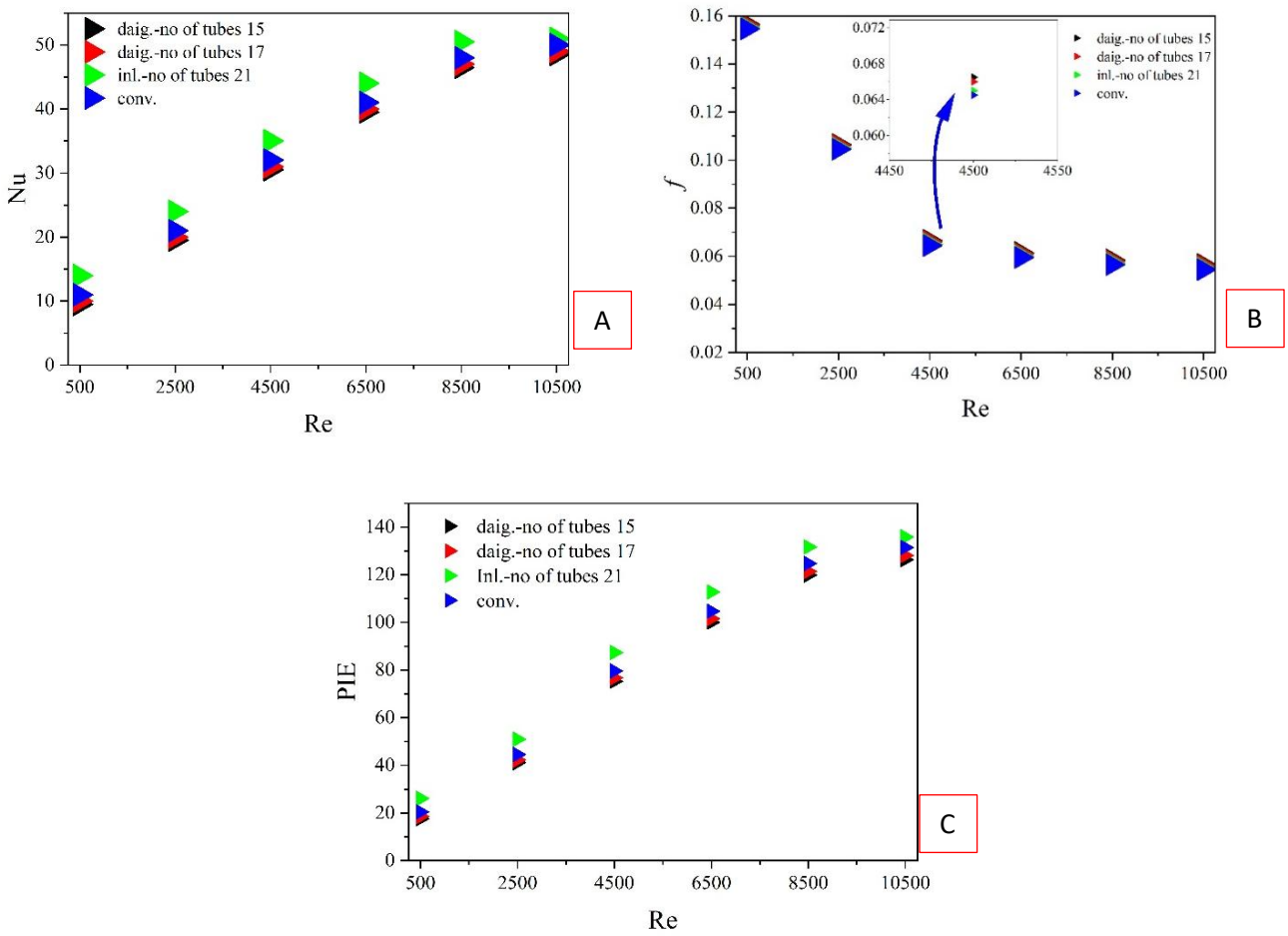

Figure 14. Effect of bypass tubes numbers and arrangement (A)Nu (B) *f* (C) PIE

3.2. Effect of bypass tubes diameter

Figure 16 examines diameter effects (D = 10, 15, 20 mm) against a conventional layout over the tested Reynolds numbers. Across the set, the 15 mm tubes achieve the highest Nu at each Re, indicating more effective boundary-layer disruption than 10 mm and 20 mm, whereas the conventional case remains the lower bound. The *f*-Re curves show the expected downward trend with a mild local feature near Re =4.5 × 10^3, plausibly reflecting shifts in secondary-flow/reattachment structure as inertia strengthens. When heat-transfer gain and pressure drop are combined, the performance index (PIE) rises with Re for every geometry. Notably, the 15 mm tubes deliver the best thermo-hydraulic payoff at higher Re with improvement of 15.47%, edging the 10 mm option with 7.58%. This is because their slightly lower *f* offsets a small Nu deficit, while the 20 mm and conventional configurations trail. In short, a Nu-optimal diameter (15 mm) and a PIE-optimal diameter (15 mm) emerge, with selection governed by whether the duty is heat-flux-limited or pumping-power-limited-an interpretation aligned with Dittus–Boelter/Gnielinski heat-transfer scaling, Blasius/Colebrook friction behavior, and standard performance-evaluation-criteria practice.

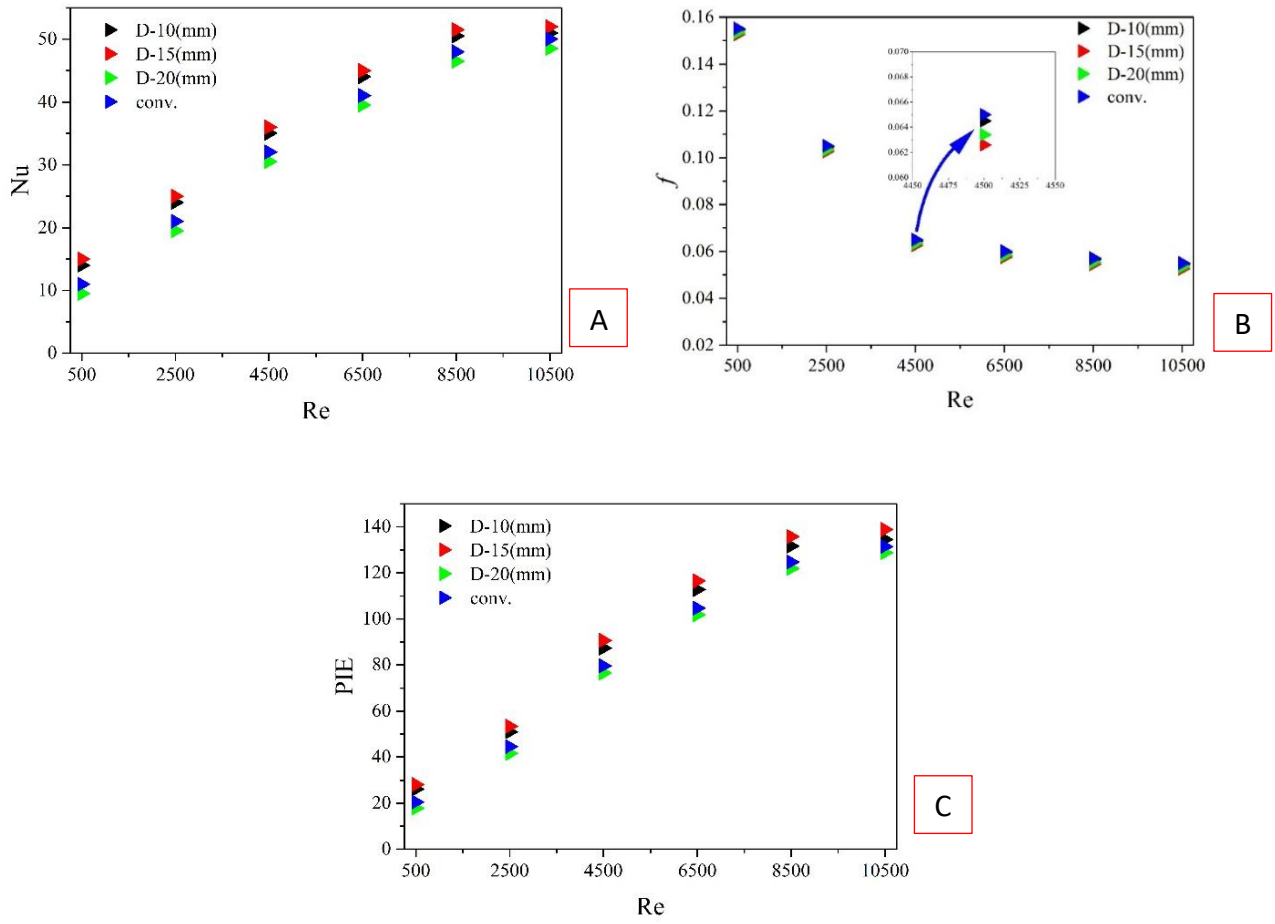

Figure 15. Effect of bypass tubes diameter (A) Nu (B) *f* (C) PIE

3.3. Effect of bypass cross section area

Figure 15 contrasts circular- and square-cross-section tube bundles with the conventional layout across Reynolds number. The cylindrical cross-section delivers the highest Nu at each Re, with improvement of 15.47%. This indicates stronger near-wall convection, whereas the square cross-section trails slightly-likely due to corner recirculation that increases wetted perimeter but does not translate to proportionate heat-transfer gain. The non-circular options carry a higher friction factor than the conventional layout, with the square section marginally above the cylindrical, reflecting the well-known pressure-loss penalty of sharp-corner ducts. When these effects are combined in the thermo-hydraulic metric (PIE), the cylindrical configuration ranks highest over the examined Re range, meaning its low pumping cost outweighs the heat-transfer gains of the shaped sections under the present definition; the conventional section follows, and the square section is lowest. These trends align with standard turbulent correlations and comparative studies of circular vs non-circular ducts.

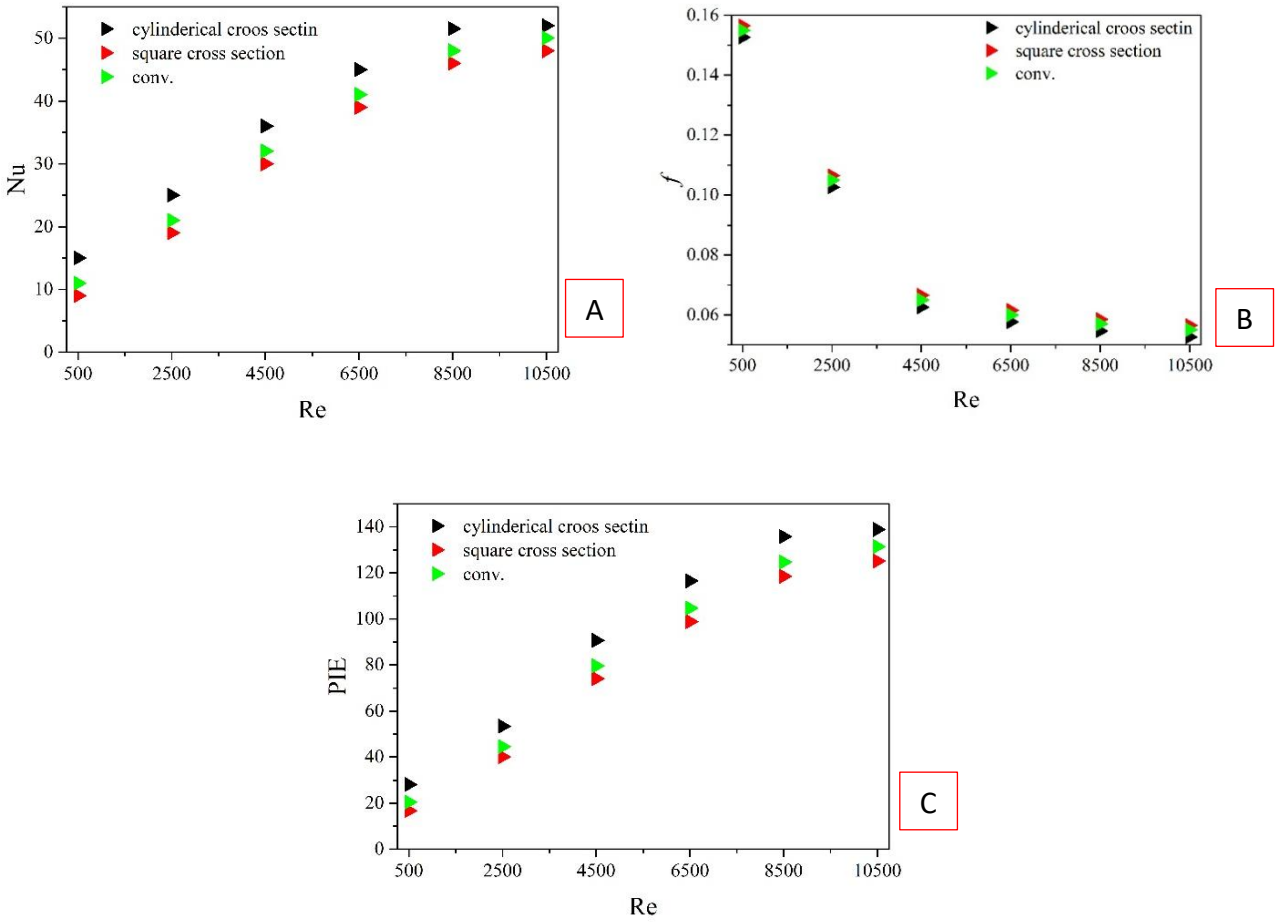

Figure 16. Effect of bypass cross section area (A) Nu (B) *f* (C) PIE

3.4. Effect of turbulator on bypass matrix

Reframing Ins-5,10,15 as turbulator inserts placed inside the bypass tube: the inserts act as flow disturbers that enhance near-wall mixing via swirl/secondary motions and repeated boundary-layer reattachment. As seen in Figure 17, they deliver modest Nu gains at low-mid Re relative to the plain bypass. But they also raise the friction factor substantially, with the ordering (*f*_Ins-5> *f*_Ins-10>*f*_Ins-15>). The local feature around that Re likely marks a change in the recirculation/reattachment pattern as the turbulator-induced vortices strengthen. When folded into the thermo-hydraulic metric, the PIE curve favors the Ins-5 at higher Re, indicating that the turbulators pumping penalty outpaces its heat-transfer benefit as inertia grows. Among the inserts, Ins-5 offers the best hydrothermal performance with 10.18% improvement, while it produces the largest pressure drop. Also, the Ins-10 produces improvement of 8.76%.

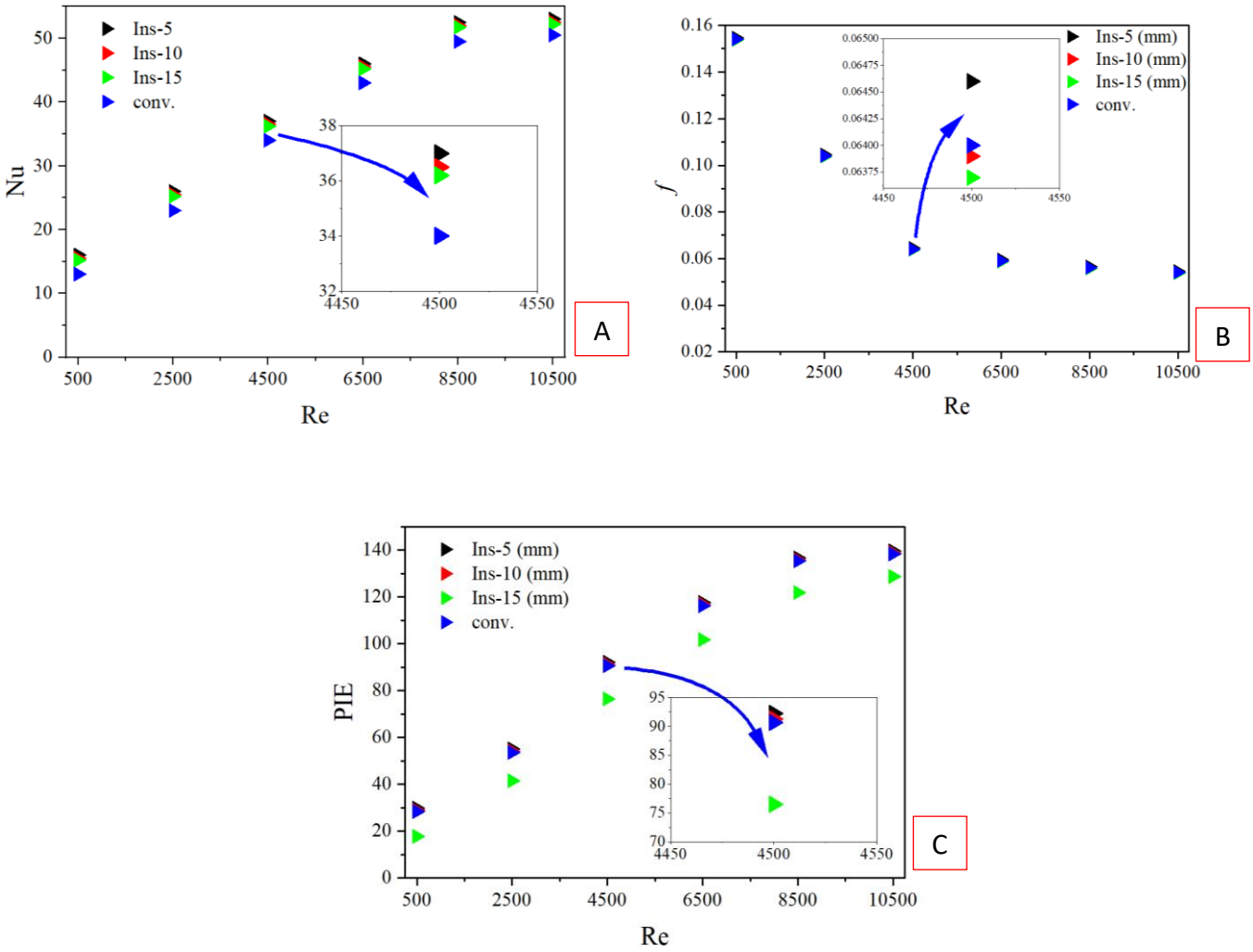

Figure 17. Effect of turbulator on bypass matrix (A) Nu (B) *f* (C) PIE

3.5. Comparison of the current work with previous studies

Lei Zhang and Defu Che [21] have conducted comprehensive experimental and numerical investigations into the thermo-hydraulic perform of CC and DU passages. The numerical model in this study was validated by selecting their experimental and numerical data as a benchmark. Figure 18 illustrates the comparison between their findings and the current data regarding j-factor and *f*. The deviations for the *f* and j factors range from -14% to 8% and from 8% to 19%, respectively. One potential explanation is that the numerical model was unable to accurately represent the anisotropic turbulence characteristics. Furthermore, the flow patterns are transitional when Reynolds number range is between 500 and 2500. Consequently, the turbulent model is unable to be completely applied to this flow pattern, resulting in a progressive decrease in the discrepancy among the numerical results and Lei zhang results as Reynolds number increased. The j factor and the friction factor are both understated by 20-30% and 20-25%, respectively, in the study conducted by Ciofalo et al. [22]. Jain et al. [23] stated that the deviations for j and *f* are less than 18% and 14.5%, respectively. The numerical model in this work is capable of addressing the current issue, as evidenced by the comparison.

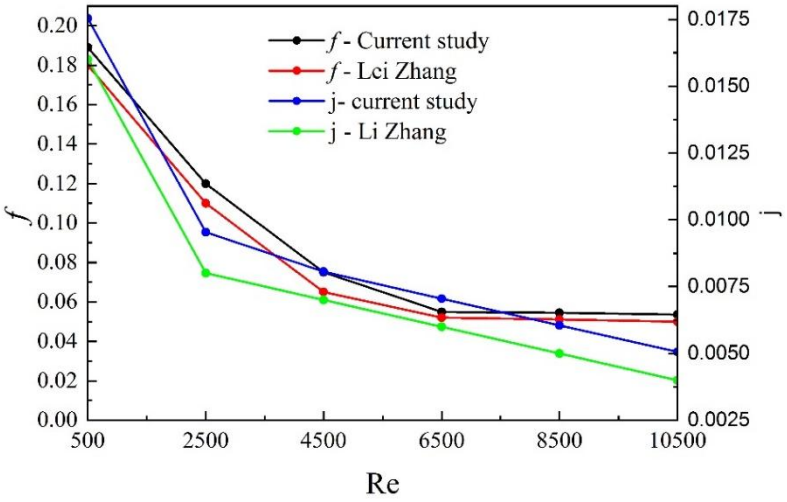

Figure 18 Comparisons of the current study with Lei zhang and Defu Che results

4. Conclusion

This study investigates the impact of geometrical parameters on the thermo-hydraulic performance of Notched Flat (NF) elements experimentally. The experimental investigations were conducted using a hot air wind tunnel specifically designed for this purpose. The preheater performance is investigated using air as working fluid with Reynold number ranged from 500 to 10500.The inlet cold side temperature is 300 k, and inlet hot side temperature is 340 k. Three bypass configurations are experimentally tested to determine the optimal arrangement and number of tubes, followed by testing bypass tubes of different diameters (10, 15, and 20 mm) and shapes (circular and square). In addition, three WCCMT turbulators of 5, 10, and 15 mm pitch were used inside the bypass tubes to promote turbulence and improve convective heat transfer. The results show that:

- Jet Impingement Effects: Bypass jets discharge into region with full temperature gradient. Collimated high-velocity jets (with velocity ratio ≈ 2–3× that of the bulk flow) impact on corrugated surfaces. Stagnation points are formed due to impingement and locally reduced thermal boundary layers.
- Wake-Induced Mixing: Organized vortex streets form downstream of each bypass tube. Von Kármán vortex shedding promotes cross-stream mixing. Flow dynamics are no longer laminar due to wake turbulence -Wake-induced mixing disrupts thermal stratification causing bulk fluid temperature uniformity. Tube-induced horseshoe vortices scour wall boundary fluid, inhibiting growth of thermal boundary layers.
- Secondary Flow Generation: Bypass tubes generate streamwise vortices pairs in corrugated channels. Secondary flow brings hot wall fluid toward core. Dean vortices (in curved flow around tubes) promote radial heat transfer. Cooperative toroidal and poloidal secondary flows driven by corrugation and tube, respectively
- The thermal-hydraulic performance of the NF heating elements with by-pass tube in the intermediate layer is more effective in terms of heat transfer rate and pressure drop. Where, the bypass matrix with inline tubes delivers an improvement of approximately 11% compared with the conventional matrix. While Notably, the 15 mm tubes deliver the best thermo-hydraulic payoff at higher Re with improvement of 15.47%, edging the 10 mm option with 7.58%. The cylindrical cross-section delivers the highest Nu at each Re, with improvement of 23.49% compared to the non-circular cross section. Among the inserts, Ins-5 offers the best hydrothermal performance with 10.18% improvement, while it produces the

largest pressure drop. While the Ins-10 produces improvement of 8.76% as compared to the conventional element.

Abbreviation		Greek symbols	
Conv.	conventional	μ	dynamic viscosity, Pa s
Ins	insertion	δ	Plate thickness
Mod.	modified	ε	dissipation, m^2/s^3
NF	Notched Flat	θ	corrugation angle
PEF	Performance Evaluation Factor	ρ	fluid density kg/ m^3
PIF	Performance Index Factor		
RAPH	Rotary air preheater		
RPM	Revolution Per Minute		
NF	Notched Flat		
		Subscripts	
Symbols			
Ac,ch	cross-sectional area of channel	f	fluid
As	Surface area	i	inlet
c	specific heat, J./kg.C	o	outlet
Dh	hydraulic diameter, mm		
f	friction factor		
h	heat transfer coefficient, W/m^2 K		
H	height of the plate, mm		
k	thermal conductivity, W/mK		
$\dot{m}$	mass flow rate,kg/s		
Nu	Nusselt number		
P	Pitch of plate (mm)		
Δp	pressure drop,pa		
Re	Reynolds number		
Tm	Mean fluid temperature, K		
Ts	Plate temperature, K		
Ac,ch	cross-sectional area of channel		

References

1. N. Ghodsipour and M. Sadrameli, "Experimental and sensitivity analysis of a rotary air preheater for the flue gas heat recovery," *Appl. Therm. Eng.*, vol. 23, no. 5, pp. 571–580, 2003, doi: 10.1016/S1359-4311(02)00226-0.
2. T. Skiepko and R. K. Shah, "A comparison of rotary regenerator theory and experimental results for an air preheater for a thermal power plant," *Exp. Therm. Fluid Sci.*, vol. 28, no. 2–3, pp. 257–264, 2004, doi: 10.1016/S0894-1777(03)00048-7.
3. E. Wang, K. Li, J. Mao, N. Husnain, D. Li, and W. Wu, "Experimental study of flow and heat transfer in rotary air preheaters with honeycomb ceramics and metal corrugated plates," *Appl. Therm. Eng.*, vol. 130, pp. 1549–1557, 2018, doi: 10.1016/j.applthermaleng.2017.11.108.
4. A. Akbari, S. Kouravand, and G. Chegini, "Experimental analysis of a rotary heat exchanger for waste heat recovery from the exhaust gas of dryer," *Appl. Therm. Eng.*, vol. 138, pp. 668–674, 2018, doi: 10.1016/j.applthermaleng.2018.04.103.
5. S. M. Hazim and M. H. Alhamdo, "Performance Enhancement for Rotary Air Preheater of a Thermal Power Plant," *J. Eng. Sustain. Dev.*, vol. 24, no. 6, pp. 57–67, 2020, doi: 10.31272/jeasd.24.6.5.

6. J. White and M. Vezza, “Multi-Objective Optimisation of Heat Transfer Elements within A Rotary Regenerative Heater,” *Proc. 8th World Congr. Momentum, Heat Mass Transf.*, pp. 1–11, 2023, doi: 10.11159/enfht23.173.
7. D. C. Li, H. Zhu, L. M. Wang, Y. He, Y. F. Bu, and D. F. Che, “Experimental and Numerical Study on Direct Leakage of Rotary Air Preheater,” *K. Cheng Je Wu Li Hsueh Pao/Journal Eng. Thermophys.*, vol. 41, no. 6, pp. 1325–1331, 2020.
8. Y. Yu, H. Di, B. Zhao, and H. Li, “Analysis of influence of ripple parameters of heat storage elements on flow and heat transfer performance,” *Therm. Sci. Eng.*, vol. 4, no. 2, p. 54, 2021, doi: 10.24294/tse.v4i2.1519.
9. Q. Zhang, F. Sun, and C. Chen, “Research on the three-dimensional wall temperature distribution and low-temperature corrosion of quad-sectional air preheater in larger power plant boilers,” *Int. J. Heat Mass Transf.*, vol. 128, pp. 739–747, 2019, doi: 10.1016/j.ijheatmasstransfer.2018.09.006.
10. L. Wang, Y. Bu, D. Li, C. Tang, and D. Che, “Single and multi-objective optimizations of rotary regenerative air preheater for coal-fired power plant considering the ammonium bisulfate deposition,” *Int. J. Therm. Sci.*, vol. 136, no. September 2018, pp. 52–59, 2019, doi: 10.1016/j.ijthermalsci.2018.10.005.
11. H. Hajebzadeh and A. N. M. Ansari, “Modification of rotary air preheater toward achieving extended life-span utilizing porous media approach: A case study,” *Proc. Inst. Mech. Eng. Part A J. Power Energy*, vol. 236, no. 2, pp. 293–307, 2022, doi: 10.1177/09576509211034977.
12. H. Abroshan and M. Goodarzi, “Optimization of a three-layer rotary generator using genetic algorithm to minimize fuel consumption,” *J. Mech. Eng. Sci.*, vol. 14, no. 1, pp. 6304–6321, 2020, doi: 10.15282/jmes.14.1.2020.09.0494.
13. J. Q. Gao and X. P. Gu, “The experimental system design on heat transfer and flow characteristics of rotary air preheater,” *Appl. Mech. Mater.*, vol. 602–605, pp. 90–93, 2014, doi: 10.4028/www.scientific.net/AMM.602-605.90.
14. I. Konovalenko, A. Ludwig, and H. Leopold, “Real-time temperature prediction in a cold supply chain based on Newton’s law of cooling,” *Decis. Support Syst.*, vol. 141, p. 113451, 2021, doi: https://doi.org/10.1016/j.dss.2020.113451.
15. Y.-T. Yang and M.-L. Hwang, “Numerical simulation of turbulent fluid flow and heat transfer characteristics in heat exchangers fitted with porous media,” *Int. J. Heat Mass Transf.*, vol. 52, no. 13, pp. 2956–2965, 2009, doi: https://doi.org/10.1016/j.ijheatmasstransfer.2009.02.024.
16. S. Hassani, R. Saidur, S. Mekhilef, and A. Hepbasli, “A new correlation for predicting the thermal conductivity of nanofluids; using dimensional analysis,” *Int. J. Heat Mass Transf.*, vol. 90, pp. 121–130, 2015, doi: https://doi.org/10.1016/j.ijheatmasstransfer.2015.06.040.
17. G. Aujla and C. Ranganayakulu, “Establishment of Colburn ‘j’ factor and Fanning friction factor ‘f’ correlations for a compact heat exchanger having perforated wavy fins using Computational Fluid Dynamics,” *Int. J. Heat Fluid Flow*, vol. 108, p. 109484, 2024, doi: https://doi.org/10.1016/j.ijheatfluidflow.2024.109484.
18. S. Kim and Y. Joo, “Energy-based key performance indicator for energy-intensive manufacturing processes: Application to steel casting,” *Energy*, vol. 317, p. 134543, 2025, doi: https://doi.org/10.1016/j.energy.2025.134543.
19. S. V Karmare and A. N. Tikekar, “Analysis of fluid flow and heat transfer in a rib grit roughened surface solar air heater using CFD,” *Sol. Energy*, vol. 84, no. 3, pp. 409–417, 2010, doi: https://doi.org/10.1016/j.solener.2009.12.011.

20. R. Mahshid, Z. Mansourvar, and H. N. Hansen, “Tolerance analysis in manufacturing using process capability ratio with measurement uncertainty,” *Precis. Eng.*, vol. 52, pp. 201–210, 2018, doi: https://doi.org/10.1016/j.precisioneng.2017.12.008.

21. L. Zhang and D. Che, “An experimental and numerical investigation on the thermal-hydraulic performance of double notched plate,” *J. Heat Transfer*, vol. 134, no. 9, pp. 1–7, 2012, doi: 10.1115/1.4006210.

22. M. Ciofalo, J. Stasiek, and M. W. Collins, “Investigation corrugated of flow and heat transfer Numerical simulations,” *Int. J. Heat Mass Transf.*, vol. 39, no. 1, pp. 165–192, 1996.

23. S. Jain, A. Joshi, and P. K. Bansal, “A new approach to numerical simulation of small sized plate heat exchangers with chevron plates,” *J. Heat Transfer*, vol. 129, no. 3, pp. 291–297, 2007, doi: 10.1115/1.2430722.